AL-ZAHRAA UNIVERSITY JOURNAL
Health and Medical Science

Al-Zahraa Journal for Health and Medical Sciences 2025; **3**:102-125 **Vol. 3, No.4, 2025**
www.zjhms.alzahraa.edu.iq

Cellulose–bentonite clay as an efficient adsorbent for Leishman dye: Investigation of Adsporption isotherm

Zahra Ridha Hassan[1], Eman Talib Kareem[1]

Department of Chemistry, College of Science, University of Kerbala, Karbala, Iraq.
* zahraaa.r@s.uokerbala.edu.iq

Received: 06 December , Year (2025), Accepted: 25 December. 2025. Published: 31 Dec. 2025

ABSTRACT

This study investigated the efficacy of adsorption for Leishman dye from aqueous solutions using a bentonite–diethylaminoethyl cellulose composite (Bt–DEAE-cellulose). The effects of adsorbent mass, contact time and acidity on dye removal were studied in a batch adsorption system. Fourier-transform infrared (FTIR) spectroscopy, scanning electron microscopy with energy-dispersive X-ray analysis (SEM/EDX), and X-ray diffraction (XRD), were used to evaluate the composite, demonstrating a mesoporous structure and effective surface modification. Dye removed almost 95% when the ideal adsorption conditions were, 0.007 g of adsorbent in 25 mL of 100 mg L^{-1} solution, 30 minutes of contact time, and pH=8. The Langmuir model yielded the greatest adsorption capacity 700 $mg.g^{-1}$, while Freundlich, Temkin, and Langmuir isotherms provided a good description of the equilibrium data. Adsorption is spontaneous and exothermic between 288 and 318 K, according to thermodynamic characteristics ($\Delta G < 0$; $\Delta H < 0$). These findings show that Bt-DEAE-cellulose is an effective and inexpensive adsorbent for handling dye-containing wastewater, including Leishman dye

Key words : Adsorption, Bentonite, DEAE-cellulose, Leishman dye.

AL ZAHRAA UNIVERSITY JOURNAL
Health and Medical Science

Al-Zahraa Journal for Health and Medical Sciences 2025; **3**:**102-125** **Vol. 3, No.4, 2025**
www.zjhms.alzahraa.edu.iq

1.Introduction

Industrial effluents continue to contain dyes because many chromophores are poisonous, persistent, and highly colored at detectable levels, endangering human health and the environment [1]. Because of its broad applicability, regenerability, and ease of operation, adsorption is a desirable treatment option for polishing diluted waste waters [2].Due to its permanent layer charge, high cation-exchange capacity, and changeable surfaces/interlayers, bentonite a smectitic aluminosilicate dominated by montmorillonite is frequently utilized as an inexpensive adsorbent [3]. By increasing area, adjusting surface charge, and creating new binding sites, chemical or polymer modifications (such as acid activation, pillaring, surfactant, or polymer intercalation) can improve capacities and kinetics [4]. Complementary clay texture ion-exchange and polymer functionality are exploited by related clay–polymer nanocomposites[5], resulting in synergistic absorption and simpler handling separation [6]. Ion exchange and multiscale binding in mixed contaminant matrices are facilitated by clay frameworks [7]. Simultaneously, cellulose-based adsorbents offer hydroxyl-rich, renewable backbones that are easily functionalized for anionic cationic dyes [8]. Recoverable cellulose composites, such as magnetic or monolithic hydrogels, reduce fine powder separation problems without sacrificing functionality [9]. Surface area, porosity, and accessible functional groups for dye capture and reuse are further improved by developments in nano-cellulose and composites [10]. In accordance with manufacturer recommendations for its working pH and cellulose matrix [11], DEAE-cellulose introduces weak-base anion-exchange sites for anion-rich systems that bind negatively charged species and can regenerate under moderate circumstances [12]. To speed up mass transfer, increase capacities, and facilitate recovery, cellulose–bentonite hybrids combine polymeric charge sites with clay exchange/texture, [13]. In order to prevent misunderstanding, current guidelines encourage rigorous model selection and validation. Robust evaluation depends on equilibrium and kinetic models [14]. The main aim of this research is to develop and characterize a diethylaminoethyl-cellulose modified Iraqi bentonite (Bt–DEAE-Cellulose) and evaluate its effectiveness for removing Leishman dye from aqueous solution by studying adsorption performance, isotherms, and thermodynamics.

IRAQI
Academic Scientific Journals

AL ZAHRAA UNIVERSITY JOURNAL
Health and Medical Science

Al-Zahraa Journal for Health and Medical Sciences 2025; 3:102-125 **Vol. 3, No.4, 2025**
www.zjhms.alzahraa.edu.iq

2.Experiment procedure

2.1.Materials

The clay sample is provided by the Baghdad, Iraq-based Company of Geological Survey and Mining. HCl and CH_3COOH, GDH, assay acidimetric 35–38%, and NaOH, Mumbai SDFCL, with a purity of 98.0%, were employed. DEAE-Cellulose supplied by B.D.H , nice chemicals Pvt. Ltd., Kochi, India is the source of Leishman dye.

2.2.Method

2.2.1. Preparation of modified clay

To create a clear, uniform polymer solution, (2.0 g) of diethylaminoethyl cellulose was dissolved in (100 mL) of 2% (v/v) acetic acid and stirred 104onstantly for one houre at 313 K. To exfoliate its layered structure, (10.0 g) of bentonite was separately dissolved in 100 mL of deionized water and agitated for an hour at 298K. To enable electrostatic interaction between the clay and cellulose, the clay suspension was then gradually added dropwise to the cellulose solution while being continuously stirred. This process was carried out for four hours at 298 K. Once the mixture had settled, 5 M NaOH was added, which change the pH from (7.2 to 8.6), which caused the DEAE-Cellulose to precipitate and create a solid-phase composite. Filtering was used to extract the resultant Bt–DEAE–Cellulose, which was then cleaned with deionized water to a pH of neutral and dried overnight at (313 K). Lastly, to create a fine powder for adsorption tests, the dry material was crushed and sieved through a (75 µm) filter.

Figure 1. Schematic diagram of Preparation of (Bt-DEAE-Cellulose) composites.

AL ZAHRAA UNIVERSITY JOURNAL
Health and Medical Science

Al-Zahraa Journal for Health and Medical Sciences 2025; 3:102-125 **Vol. 3, No.4, 2025**
www.zjhms.alzahraa.edu.iq

2.2. Preparation of Leishman Solution

The stock solution of leishman stain (200 mg.L^{-1}) was generated by immersing 0.02 g in 100 mL of purified water, and dyes experimental concentration was reached by gradually diminishing the solution with distilled water .

3.Batch Experiment

Through batch studies, the adsorption capabilities of modified bentonite-cellulose (Bt–DEAE–Cellulose) for the elimination of Leishman dye from aqueous solutions were assessed. Important operational factors were examined to determine their impact on adsorption effectiveness, such as pH (2–10), contact period (5–120 min), and adsorbent dosage (0.001–0.05 g). In each experiment, 0.007 g of the modified adsorbent was used under controlled circumstances to stir a set amount (25 mL) of dye solution. Using the following formula, the adsorption capacity (Q_e, mg/g) was determined[15]:

$$Qe = \frac{v(C_o - C_e)}{m} \qquad (1)$$

Where C_o= starting concentration mg.L^{-1}. C_e = concentration of Leishman dye at equibrium mg.L^{-1}, m = the mass of the adsorbent g and V = volume of solution L .

The percentage of dye removal **(**%R**)** was also determined using[15]:

$$\%R = \frac{(C_o - C_e)}{C_o} \times 100 \qquad (2)$$

3. Results and discussion

3.1 Characterization of Clay Composite :

3.1.1. FT-IR Analysis:

The FTIR spectrum of bentonite clay recorded in the range 4000 to 400 cm^{-1} is shown in Figure 2. Natural bentonite's FTIR spectrum demonstrates the characteristics of a hydrated smectite aluminosilicate. The stretching vibration of structural hydroxyls (Al–Al–OH) is shown by the strong band at (3626.29 cm^{-1}), whereas the bending vibration of same hydroxyl groups is represented by the weaker band at 918.15 cm^{-1}. The stretching and bending vibrations of

IRAQI Academic Scientific Journals

AL ZAHRAA UNIVERSITY JOURNAL
Health and Medical Science

Al-Zahraa Journal for Health and Medical Sciences 2025; **3**:102-125 **Vol. 3, No.4, 2025**
www.zjhms.alzahraa.edu.iq

interlayer / adsorbed water are responsible for the large absorption at (3410.26 cm^{-1}) and the band at (1641.48 cm^{-1}), indicating that the clay is hydrated [16]. Si–O stretching in the tetrahedral silicate framework is linked to a strong band at 1039.67 cm^{-1}, whereas Si–O–Al and Si–O–Si bending modes are connected with low-wavenumber bands at (524.66 and 470.65 cm^{-1}), respectively [17]. Al–Fe–OH and Al–Mg–OH vibrations are responsible for additional bands at 833.28 and 796.63 cm^{-1}, which are compatible with small octahedral replacements. When taken as a whole, these absorptions support the usual layered smectite (bentonite) structure, which is dominated by interlayer water, structural hydroxyls, and silicate framework vibrations [18].

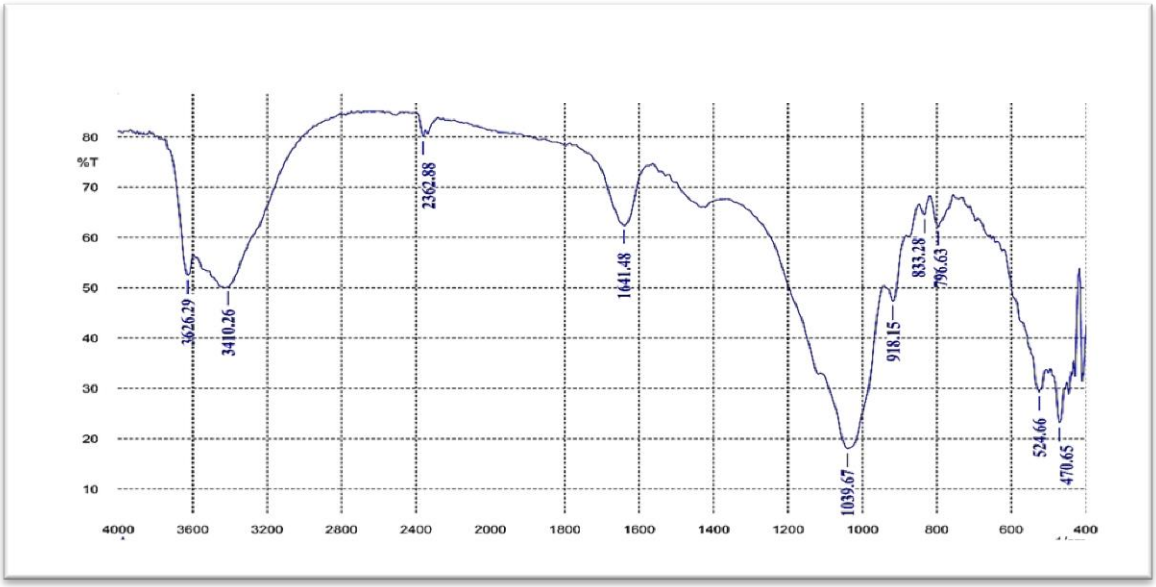

Figure 2. FT-IR spectrum for Natural Bentonite.

DEAE-Cellulose's FT-IR spectra shows(Figure 3) distinctive peaks that attest to its functional groups. O–H stretching vibrations from hydroxyl groups, which are prevalent in the cellulose backbone, are responsible for a large and powerful absorption band at (3398.76 cm^{-1}) [19]. In aliphatic -CH_2- groups, the peak at (2899.11 cm^{-1}) is associated with C–H stretching. Water absorbed in the polymer matrix is probably the cause of the (1641.48 cm^{-1}) peak, which shows H–O–H bending [20]. The presence of ether links in the cellulose structure is confirmed by peaks at (1371.48 cm^{-1}) and (1155.40 cm^{-1}), which are indicative of C–H bending and C–O–C asymmetric stretching, respectively [21].The C–O and C–O–C stretching vibrations, which are

IRAQI Academic Scientific Journals

AL ZAHRAA UNIVERSITY JOURNAL
Health and Medical Science

Al-Zahraa Journal for Health and Medical Sciences 2025; 3:102-125 **Vol. 3, No.4, 2025**
www.zjhms.alzahraa.edu.iq

common in polysaccharides, are further supported by the strong band at (1024.24 cm^{-1}). All things considered, these spectrum characteristics support DEAE-Cellulose's chemical makeup and aptitude for clay surface modification[22].

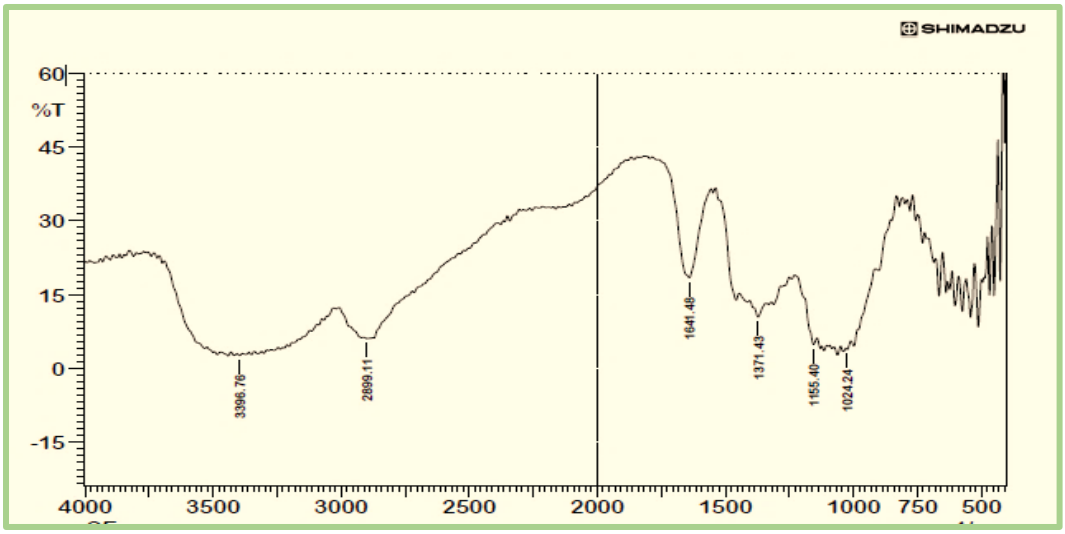

Figure 3. FT-IR spectrum for DEAE-Cellulose.

A number of absorption bands in the Bt–DEAE–Cellulose composite's FT-IR spectra (as shown in Figure 4) attest to the bentonite's effective alteration with DEAE–Cellulose. The C–H stretching vibrations of the aliphatic $–CH_2–$ groups from the cellulose chains are responsible for the peaks at 2918.40 cm^{-1} and 2850.98 cm^{-1} [23]. Weak C–H aromatic or –CH=CH– stretching may be represented by a faint but discernible band at 3014.64 cm^{-1}, which might suggest a little structural rearrangement. The $–CH_2$ bending is represented by a prominent absorption band at 1475.69 cm^{-1}, and the C–O–C stretching vibrations characteristic of cellulose ether linkages are linked to the peak at 992.51 cm^{-1} [24]The existence of bentonite's silicate framework is suggested by the peak at 727.19 cm^{-1}, which is frequently associated with Si–O or out-of-plane C–H bending. Together, these characteristics show that DEAE–Cellulose was able to adhere to the surface of bentonite, creating a hybrid organic–inorganic material with active functional groups that is perfect for adsorption uses.

IRAQI Academic Scientific Journals

AL ZAHRAA UNIVERSITY JOURNAL
Health and Medical Science

Al-Zahraa Journal for Health and Medical Sciences 2025; 3:102-125 **Vol. 3, No.4, 2025**
www.zjhms.alzahraa.edu.iq

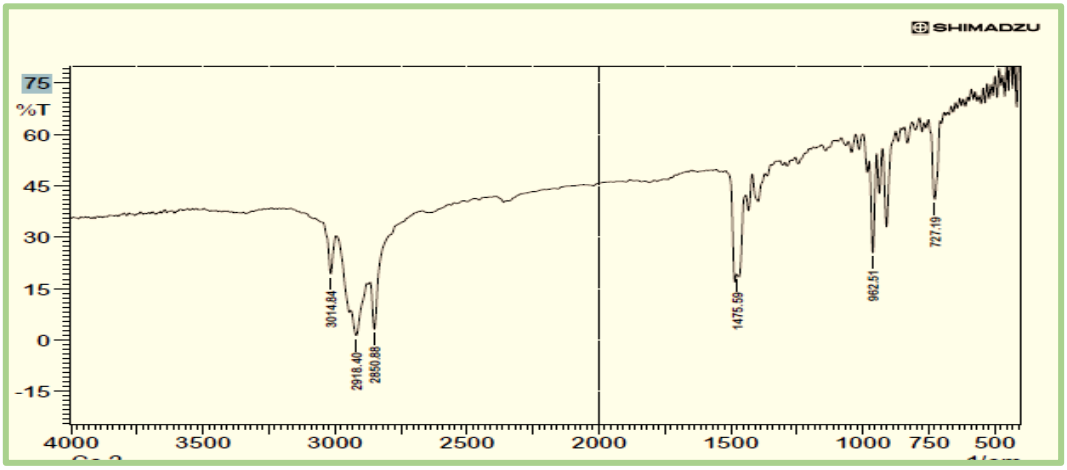

Figure 4. FT-IR spectrum for Bt-DEAE-Cellulose

3.1.2.SEM Analysis

The Bt–DEAE–Cellulose SEM picture at 20,000 magnification (as in Figure 5) .Figure5 shows layered, uneven clay sheets embedded with rod-like and fibrous structures, indicating that the DEAE–Cellulose surface modification was effective. These projections imply a robust interaction between the negatively charged clay surfaces and the cationic cellulose, which is in line with earlier research on organic–inorganic hybrid adsorbents [25][26]. Improved surface area and active site accessibility are indicated by the increased surface roughness and porous morphology, both of which are essential for adsorption effectiveness [27]. The effective creation of a composite structure appropriate for dye adsorption is further validated by the presence of cellulose-associated textures and the fracturing of the compact clay matrix [28].

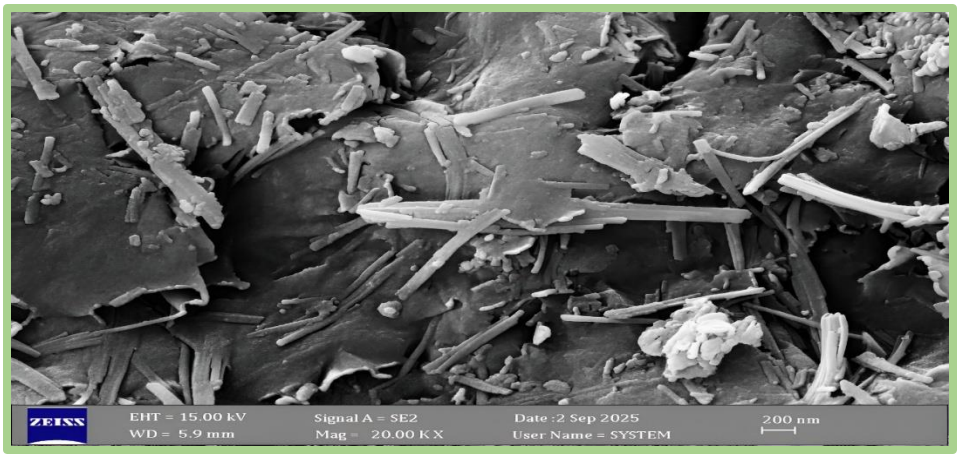

Figure 5. SEM Image for Bt-DAEA-Cellulose.

IRAQI Academic Scientific Journals

AL ZAHRAA UNIVERSITY JOURNAL
Health and Medical Science

Al-Zahraa Journal for Health and Medical Sciences 2025; 3:102-125 **Vol. 3, No.4, 2025**
www.zjhms.alzahraa.edu.iq

3.1.3 Energy Dispersive X-ray Spectroscopy (EDX).

The Bt–DEAE–Cellulose composite's successful creation is confirmed by the EDX spectrum (illustrated in Figure 6) . The aluminosilicate structure of bentonite and the cellulose modifier combine to form major components including O (30.2%), Si (28.5%), and C (20.9%) [29] . The mineral composition of natural clay is indicated by the presence of Al (9.3%), Fe (5.4%), Ca (2.4%), Mg (2.1%), and Na (1.3%) [30]. The incorporation of cellulose is further supported by the high oxygen and carbon content. Sputter coating during SEM processing produces gold (Au) peaks. A hybrid organic–inorganic adsorbent structure is confirmed by these data, which also corroborate FTIR and SEM observations [31].

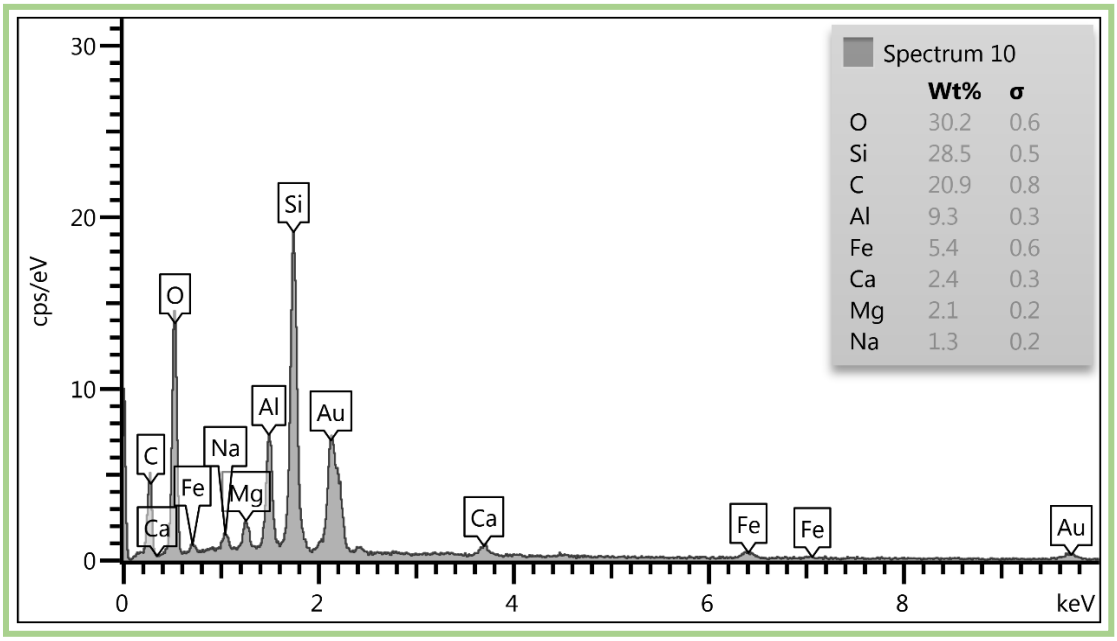

Figure 6. EDX Image for Bt-DAEA-Cellulose

3.1.4. XRD Diffraction spectroscopy Analysis.

The XRD patterns of the BT–DEAE–cellulose composite and raw bentonite are compared in Figures 7A and B and Table 1. The montmorillonite-related basal peak arises at 2θ = 20.92° (d = 4.433 Å) in the natural clay's distinctive smectite/aluminosilicate reflections [32]. This reflection changes to 2θ = 19.32° (d = 4.589 Å) after treatment with DEAE–cellulose, indicating an increase in basal spacing of Δd ≈ +0.156 Å. This extension supports the successful intercalation of DEAE–cellulose chains into the bentonite interlayer galleries and shows a partial disruption of the initial layer stacking [33]. Furthermore, quartz impurities that were first detected at 26.77° (d

IRAQI Academic Scientific Journals

AL ZAHRAA UNIVERSITY JOURNAL
Health and Medical Science

Al-Zahraa Journal for Health and Medical Sciences 2025; 3:102-125 **Vol. 3, No.4, 2025**
www.zjhms.alzahraa.edu.iq

= 3.327 Å) and 39.53° (d = 2.277 Å) are still present after alteration, showing up with just minor shifts at 26.20° (d = 3.398 Å) and 39.06° (d = 2.304 Å). These reflections' retention implies that the crystalline quartz phase is not substantially changed by the intercalation/functionalization process[34]. In contrast, the calcite peak in the natural clay, which is centered at 29.48° (d = 3.026 Å), becomes weaker and slightly moved to 28.24° (d = 3.157 Å) in the composite[35]. This might be explained by weak interactions between the carbonate components and the functional groups of DEAE–cellulose [36]. The creation of the BT–DEAE–cellulose clay–polymer nanocomposite with changed structural and surface properties is confirmed by the overall drop in peak intensities and the slight widening of reflections in the modified sample, which show reduced crystallinity and structural rearrangement.

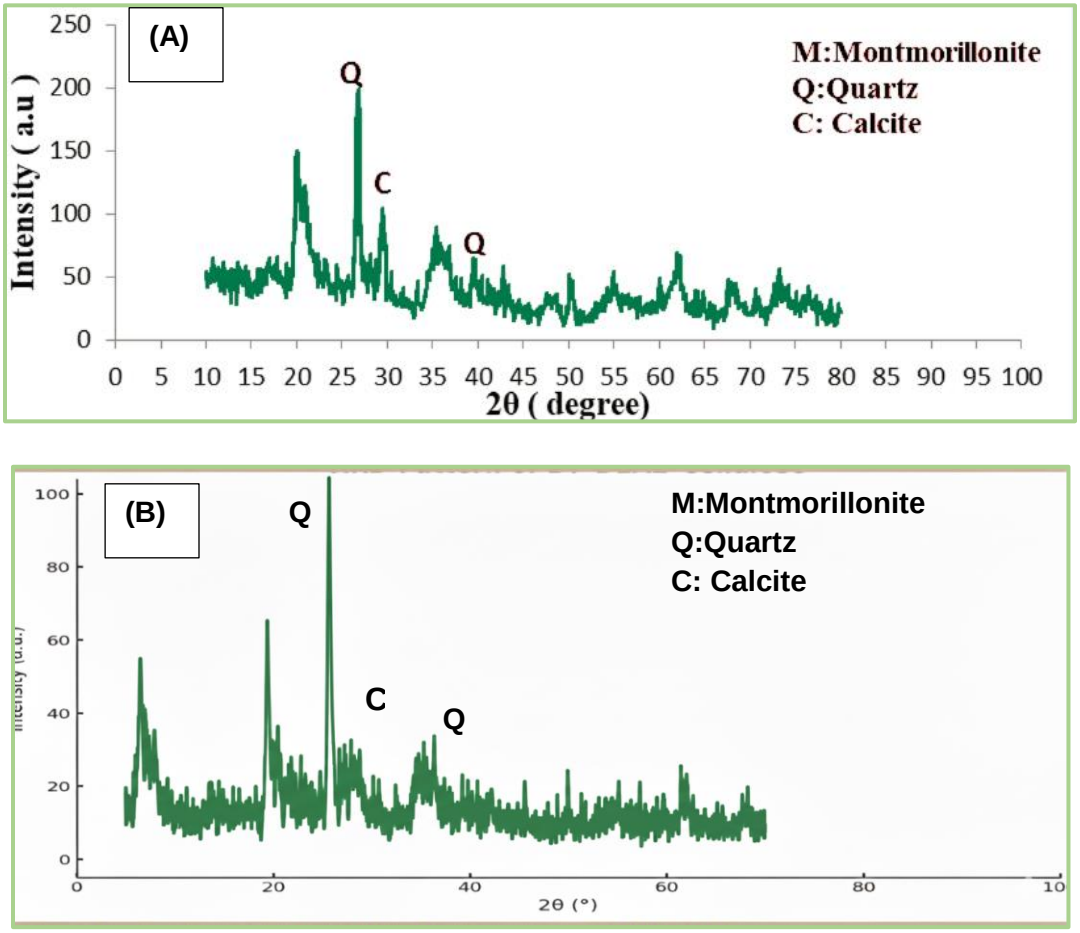

Figure7. A)XRD Pattern for natural clay sample B) XRD Pattern of modified clay sample

AL ZAHRAA UNIVERSITY JOURNAL
Health and Medical Science

Al-Zahraa Journal for Health and Medical Sciences 2025; 3:102-125 Vol. 3, No.4, 2025
www.zjhms.alzahraa.edu.iq

Table 1 Comparative XRD analysis of raw Bentonite clay and modified clay sample

Bentonite clay					BT–DEAE–Cellulose clay				
2-Theta	**d (Å)**	**Height**	**I %**	**FWHM**	**2-Theta**	**d (Å)**	**Height**	**I %**	**FWHM**
20.92	4.433	65	32.7	0.414	19.325	4.589	10	52.5	0.368
26.77	3.327	199	100	0.356	26.205	3.398	14	100	0.198
39.53	2.277	65	32.7	0.381	39.061	2.304	9	19.2	0.099
29.48	3.026	104	52.3	0.377	28.248	3.157	20	28.3	0.085

3.1.5 Brunauer-Emmet-Teller (BET) Scans

According to the BET theory- the modified Bt-DAEA_Cellulose's BET surface area and pore size distribution were assessed using the nitrogen adsorption-desorption isotherm. The adsorption-desorption curve displays a type IV isotherm, which is typical of mesoporous materials- as seen in Figure 8A. The hysteresis loop, which is of type H3- shows slit-shaped pores created by the aggregation of plate-like particles in the relative pressure (P/P_0) range of 0.3–1.0.[37]. Mesopores are confirmed by the Barrett-Joyner-Halenda (BJH) pore size distribution seen in Figure 8B. According to the BET study, the modified Bt-DAEA Cellulose has an average pore diameter of 19.563 nm, a specific surface area of 22.666 m^2g^{-1}, and a total pore volume of (5.9778 $cm^3.g^{-1}$). According to these findings, the material is classified as mesoporous (2–50 nm), which is in line with the anticipated structure of modified adsorbents based on cellulose [38].

IRAQI Academic Scientific Journals

AL ZAHRAA UNIVERSITY JOURNAL
Health and Medical Science

Al-Zahraa Journal for Health and Medical Sciences 2025; 3:102-125 **Vol. 3, No.4, 2025**
www.zjhms.alzahraa.edu.iq

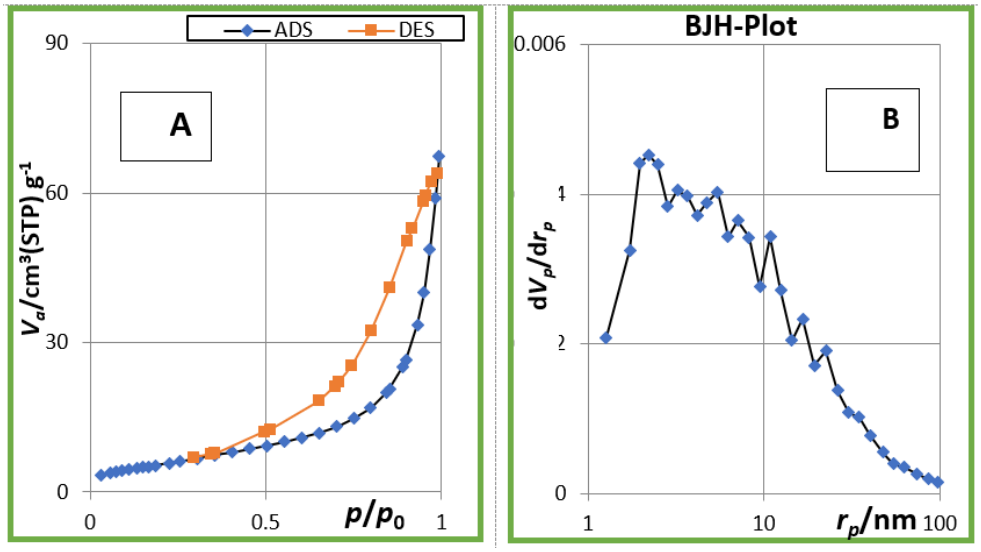

Figure 8 A: N_2 adsorption- desorption Isotherms of modified Bt-DAEA_Cellulose, B: The Corresponding Barrett-Joyner-Halenda pore size distribution curve .

3.2 Adsorption of Leishman dye on Bt-DEAE-Cellulose surface

3.2.1 Effect of adsorbent dosage

At pH = 8 and an initial concentration C_0 = 100 mg·L^{-1} as demonstrated in Figure 9, this impact was investigated at 298 K. The removal increased from (67.7% at 0.001 g) to (93.6% at 0.007 g). However, no further rise was detected beyond this threshold (0.03–0.05 g) (≈95.2%–95.5%). As the dosage increases, a greater exterior surface area is available for dye absorption, and there are more accessible exchangeable sites, which accounts for the initial steep increase [39]. When the solution becomes solute-limited and the particles crowd after achieving the critical dosage (the plateau begins at around 0.010 g), boundary layers overlap and the active sites are underutilized; as a result, the removal percentage levels off while mass-based capacity *e*q usually falls [40].Removal increased with adsorbent dosage, reaching ≈93.6% at 0.007 g. Above ≈0.010 g, the efficiency plateaued due to solute limitation and particle crowding.

IRAQI Academic Scientific Journals

AL ZAHRAA UNIVERSITY JOURNAL
Health and Medical Science

Al-Zahraa Journal for Health and Medical Sciences 2025; 3:102-125 **Vol. 3, No.4, 2025**
www.zjhms.alzahraa.edu.iq

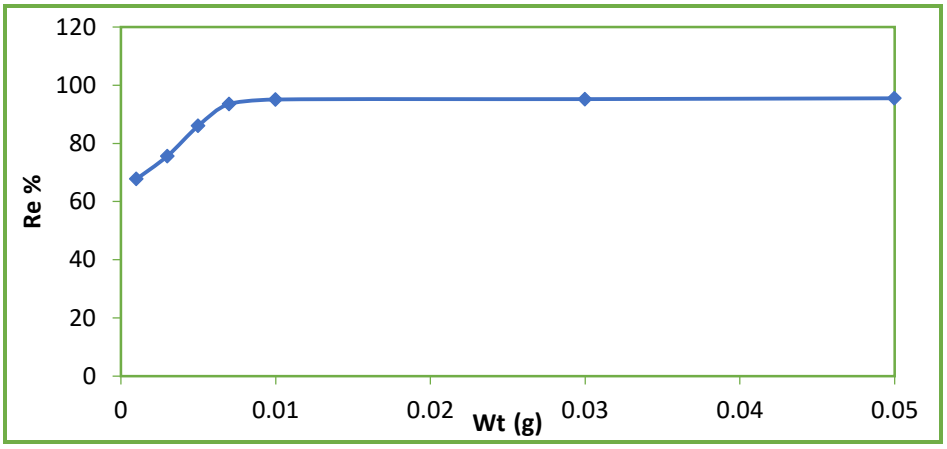

Figure 9. The effect of adsorbent dosage on the adsorption of Leishman dye at 298 K and pH **8**

3.2.2 Effect of contact time

This parameter was measured using the optimum dosage at (pH = 8), temperature 298 K, and beginning dye concentration 100 mg·L^{-1}. As seen in Figure 10, the data reveal that Leishman dye clearance rises with time before leveling off: 57.9% (5 min) → 81.5% (20 min) → ≈95.1% (30 min). Only slight changes thereafter take place (≈96–97% at 60–90 min; 96.0% at 120 min). Strong concentration gradients that promote external-film uptake and a large number of accessible binding sites are reflected in the quick early stage [41]. The adsorption capacity becomes almost constant during the equilibrium period (about 30 minutes for this modified clay), when there are fewer active sites left and mass transfer moves toward intraparticle diffusion [42]. Removal increased rapidly with contact time, reaching ≈95.1% within 30 min, then showed only minor changes up to 120 min. This indicates fast initial uptake followed by equilibrium as active sites become limited and diffusion control increases.

AL ZAHRAA UNIVERSITY JOURNAL
Health and Medical Science

Al-Zahraa Journal for Health and Medical Sciences 2025; 3:102-125 **Vol. 3, No.4, 2025**
www.zjhms.alzahraa.edu.iq

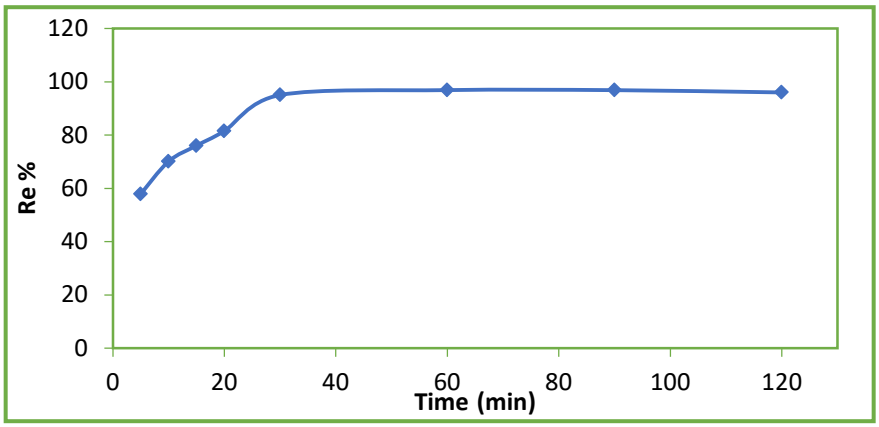

Figure 10 . Effect of Contact time on the adsorption of Leishman dye at 298 K and pH =8.

3.2.3 Effect of acidity

The solution including the clay sample and dye at 298 K and an initial concentration of 100 $mg.L^{-1}$ was mixed with a few drops of 0.1 M NaOH and HCl to measure acidity parameter, At pH=2- there was very little dye loss; it increased steadily until it reached pH =8, at which time there was no noticeable difference. For this reason, in particular, pH eight was thought to be the best for further testing, Figure 11 demonstrated this parameter Electrostatic interactions play a major role in the adsorption process based on the reported increase in adsorption with pH. In aqueous solution, Leishman dye mostly exhibits basic (cationic) dye behavior. Lower removal results from H^+ ions competing with dye cations for the available adsorption sites on the adsorbent surface, which is more protonated and/or less negatively charged at low pH. Deprotonation of surface functional groups raises the negative charge density on the clay surface as pH rises, strengthening electrostatic attraction to the cationic dye species and boosting adsorption. Adsorption sites are getting close to saturation and the system is moving toward equilibrium, as shown by the plateau above pH ≈ 8.

IRAQI Academic Scientific Journals

AL ZAHRAA UNIVERSITY JOURNAL
Health and Medical Science

Al-Zahraa Journal for Health and Medical Sciences 2025; 3:102-125 **Vol. 3, No.4, 2025**
www.zjhms.alzahraa.edu.iq

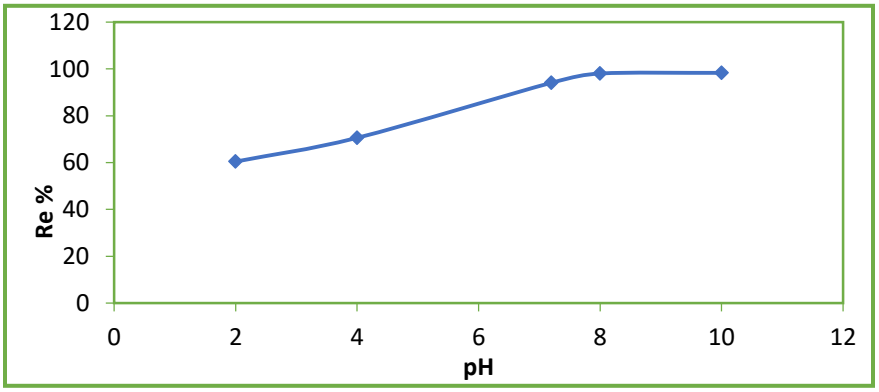

Figure 11 . Effect of pH **on adsorption of Leishman dye at 298K**.

3.2.4 Effect of temperature

The study examined how temperature affect the adsorption process ,calculating thermodynamic function such as ΔG, ΔH, and ΔS To determine the process feasibility and nature. Its possible to calculate Gibbs energy by equation below[43]:

$$\Delta G = -RT ln\, k_{eq} \qquad (3)$$

Where: ΔG = energy change kJ. mol^{-1} , R = gas constant 8.314 J. mol^{-1}. K^{-1} ,T = temperature in K.

The equilibrium constant (k_{eq}) was calculated from the following equation:

$$k_{eq} = \frac{m \cdot Qe}{v \cdot c_e} \qquad (4)$$

ΔH can be obtained from the slope and intercept the plot of Ln k_{eq} versus 1/T, Figure12, shows the plot of Leishman dye on modified clay

$$\ln k_{eq} = \frac{-\Delta H}{RT} + con \qquad (5)$$

The chang in randomness was determined from Helmholtz-Gibbs equation[44]

$$\Delta S = \frac{\Delta H - \Delta G}{T} \qquad (6)$$

IRAQI Academic Scientific Journals

AL ZAHRAA UNIVERSITY JOURNAL
Health and Medical Science

Al-Zahraa Journal for Health and Medical Sciences 2025; 3:102-125 **Vol. 3, No.4, 2025**
www.zjhms.alzahraa.edu.iq

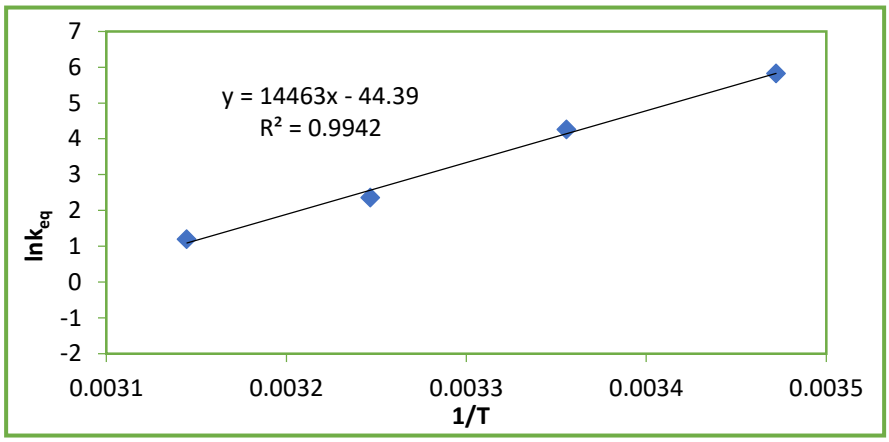

Figure 12. A plot of ln k_{eq} versus 1/T of Leishman dye adsorption on modified clay

Table 2. Thermodynamic function ΔG, ΔS and ΔH of Leishman dye adsorption on modified clay at (288-318)K.

T (K)	-ΔG (KJ/mol)	ΔH (KJ/mol)	ΔS (J/mol.k)
288	**-13.9334**	**-120.2450**	**-369.1390**
298	**-10.5618**		**-368.0660**
308	**-6.0222**		**-370.8540**
318	**-3.1654**		**-368.1760**

3.3 Adsorption equilibrium isotherm

Different isotherm model including Langmuire, Frendlich,and Temkin were applied to correlate the adsorption capacity and residual adsorbate concentration.

3.3.1 Langmuir adsorption model

The development of a monolayer of adsorbate molecules on the surface of an adsorbent is quantitatively described by the Langmuir adsorption isotherm. It is predicated on the idea that adsorption takes place at certain homogenous sites inside the adsorbent and that, once a site is occupied, no further adsorption may occur there. The equilibrium connection between the

IRAQI Academic Scientific Journals

AL ZAHRAA UNIVERSITY JOURNAL
Health and Medical Science

Al-Zahraa Journal for Health and Medical Sciences 2025; 3:102-125 **Vol. 3, No.4, 2025**
www.zjhms.alzahraa.edu.iq

quantity adsorbed onto the solid surface and the concentration of adsorbate in the liquid phase is represented by the model [45]. The Langmuir equation's linearized form may be written as follow :

$$\frac{Ce}{Qe} = \frac{1}{ab} + \frac{Ce}{a} \qquad (7)$$

where an is the Langmuir binding constant associated with the binding sites' affinity (L/mg), and b is the maximal adsorption capacity that corresponds to monolayer coverage (mg/g). The slope $(1/a)$ and intercept $(1/ab)$ of the linear plot of Ce may be used to calculate the parameters a and b. The Ce/Qe in contrast to Ce[46] ,as proved in Figure 13.

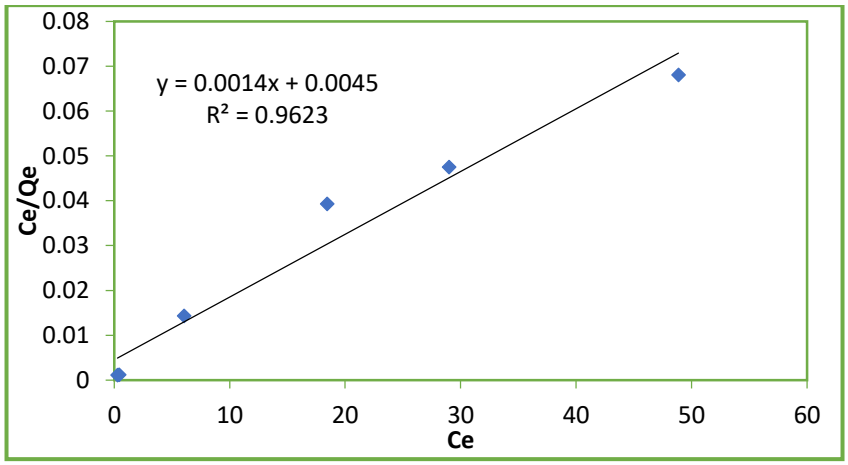

Figure 13 . Langmuire isotherm for adsorption of Leishman dye on the surface of modified clay at 298K.

3.3.2 Freundlich adsorption model

The logarithmic (linearized) form of the Freundlich isotherm, which is frequently used to explain adsorption on energetically heterogeneous surfaces and frequently yields acceptable empirical fits across a variety of sorbate–sorbent systems [47].

$$\ln qe = lnkf + \frac{1}{n} \ln Ce \qquad (8)$$

where qe The is the equilibrium amount adsorbed, Ce is the concentration at equilibrium, K_F is a capacity-related constant, while adsorption intensity /heterogeneity is expressed as $1/n$ [48].

IRAQI Academic Scientific Journals

AL ZAHRAA UNIVERSITY JOURNAL
Health and Medical Science

Al-Zahraa Journal for Health and Medical Sciences 2025; 3:102-125 **Vol. 3, No.4, 2025**
www.zjhms.alzahraa.edu.iq

Figure 14 shows the Freundlich isotherm for adsorption of Leishman dye on the surface of clay. Principles Favorable (normal) adsorption is indicated by $1/n<1$ concentration-independent (roughly linear) partitioning is indicated by $1/n\approx1$ and cooperative adsorption behavior is suggested by $1/n>1$.

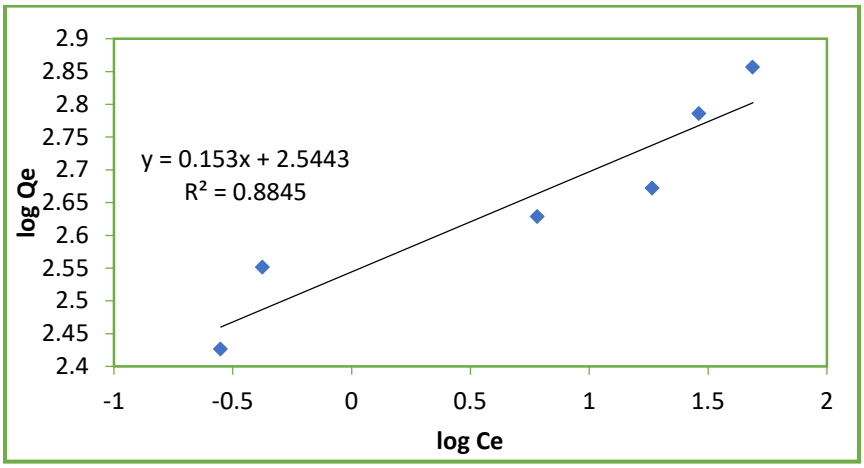

Figure 14 . Freundlich isotherm for adsorption of Leishman dye on the surface of modefied clay at 298K.

3.3.3 Temkin adsorption model

The Temkin isotherm posits that the heat of adsorption decreases linearly with surface coverage and takes adsorbate–adsorbent interactions into consideration [49]which was provied in figure 15. In its linear version

$$q_e = \frac{RT}{b_T}\ln(A_T C_e) \qquad (9)$$

where A_T is the Temkin equilibrium binding constant, and b_T is a constant associated with the heat of adsorption. [50].

IRAQI Academic Scientific Journals

AL ZAHRAA UNIVERSITY JOURNAL
Health and Medical Science

Al-Zahraa Journal for Health and Medical Sciences 2025; 3:102-125 **Vol. 3, No.4, 2025**
www.zjhms.alzahraa.edu.iq

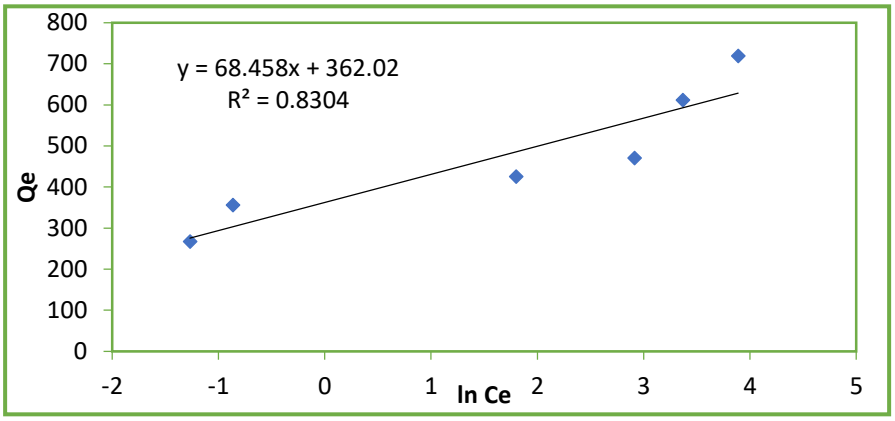

Figure 15 . Temkin isotherm for adsorption of Leishman dye on the surface of modified clay at 298K.

To interpret the adsorption equilibrium, the experimental data were fitted to Langmuir, Freundlich, and Temkin isotherm models at different temperatures. The calculated constants and correlation coefficients (R^2) are summarized in Table 3.

Table 3 Langmuir, Freundlich , and Temkin isotherm parameters for adsorption of Leishman dye on the surface of modified clay at 298K.

T(K)	Langmuir isotherm				Freundlich isotherm		
	a(mg/g)	**b(mg/L)**	**R_L**	**R^2**	**K_F (mg/g)**	**n**	**R^2**
288	500	0.3125	0.0310	0.9623	245.1319	6.5359	0.8845
298	500	0.3125	0.0310	0.9566	187.0250	4.7147	0.9130
308	588.2353	0.2656	0.0362	0.9088	67.5927	2.2431	0.9555
318	1111.1110	0.1406	0.0663	0.3921	12.1674	1.3289	0.9266

T(K)	Temkin isotherm		
	b_T	**A_T (L/mg)**	**R^2**
288	47.9210	197.9626	0.8304
298	65.0550	13.7568	0.8678
308	127.8400	2.3874	0.9020
318	177.0100	12.3435	0.8581

AL ZAHRAA UNIVERSITY JOURNAL
Health and Medical Science

Al-Zahraa Journal for Health and Medical Sciences 2025; **3**:**102-125** **Vol. 3, No.4, 2025**
www.zjhms.alzahraa.edu.iq

4. Conclusion

1. The bentonite–diethylaminoethyl cellulose composite known as Bt–DEAE-cellulose was successfully created and showed excellent efficiency in eliminating Leishman dye from aqueous solution.
2. The dye removal achieved around 95% under ideal working circumstances (0.007 g adsorbent in 25 mL of 100 mg L^{-1} dye solution, pH = 8, and 30 min contact time at about 298 K), suggesting quick absorption at a low adsorbent dosage.
3. Effective surface modification and the creation of an organic–inorganic hybrid structure with enhanced surface texture and accessible functional groups, enhancing adsorption performance, were validated by material characterisation (FTIR, SEM/EDX, and XRD).
4. The Langmuir isotherm best explained the equilibrium results, indicating mostly monolayer adsorption on energetically similar sites with favorable separation factors ($R_L < 1$) at all investigated temperatures.
5. Thermodynamic results showed spontaneous and exothermic adsorption over 288–318 K ($\Delta G < 0$; $\Delta H < 0$), supporting the feasibility of the process
6. With all factors considered, Bt-DEAE-cellulose is a promising inexpensive adsorbent for dye-contaminated water. Tests for regeneration and reusability as well as validation using actual wastewater matrices should be part of future research to verify performance in real-world scenarios.

5. Acknowledgment

The authors would like to thank all supported professors of department of chemistry, University of Karbala and Phi Center For Nanoscience

References

1. Lin, J., Ye, W., Xie, M., Seo, D.H., Luo, J., Wan, Y. and van der Bruggen, B. (2023). Environmental impacts and remediation of dye-containing wastewater. *Nature Reviews Earth & Environment*, 4, 785–803. https://doi.org/10.1038/s43017-023-00489-8.
2. Liu, H., Zhou, H. and Wang, S. (2021). Removal of heavy metals and dyes by clay-based adsorbents: From natural clays to modified nano-clays—a review. *Chemical Engineering Journal*, 420, 127574. https://doi.org/10.1016/j.cej.2020.127574.

AL ZAHRAA UNIVERSITY JOURNAL
Health and Medical Science

Al-Zahraa Journal for Health and Medical Sciences 2025; **3**:**102-125** **Vol. 3, No.4, 2025**
www.zjhms.alzahraa.edu.iq

3. Ikhsan, N., Lai, S. and Ooi, B.S. (2022). Insights on applications of bentonite clays for the removal of dyes and heavy metals from wastewater: A review. *Environmental Science and Pollution Research*, 29, 46405–46428. https://doi.org/10.1007/s11356-022-24277-x.
4. Raza, J.R., Javed, M. and Rehman, F. (2022). Adsorption of organic water pollutants by clays and clay minerals composites: A review. *Applied Clay Science*, 229, 106686. https://doi.org/10.1016/j.clay.2022.106686.
5. Singh, K.P., Ray, S.S. and Saha, B.S. (2023). Clay–polymer nanocomposites for water and wastewater treatment: A review. *Chemosphere*, 307, 135869. https://doi.org/10.1016/j.chemosphere.2022.135869.
6. Mokhtar, A., Asli, B., Abdelkrim, S., Hachemaoui, M., Boukoussa, B., Sassi, M., Viscusi, G. and Abboud, M. (2024). Polymer/clay nanocomposites as advanced adsorbents for textile wastewater treatment. *Minerals*, 14(12), 1216. https://doi.org/10.3390/min14121216.
7. dos Santos, F.F., da Silva, A.M. and Assis, J.M. (2024). Clay-based materials for heavy metals adsorption: Mechanisms and applications. *Crystals*, 14(12), 1046. https://doi.org/10.3390/cryst14121046.
8. Sharma, M., Chandra, P. and Kumar, R. (2023). Cellulose-based materials and their adsorptive removal efficiency for dyes: A review. *International Journal of Biological Macromolecules*, 224, 1337–1355. https://doi.org/10.1016/j.ijbiomac.2022.10.220.
9. Xu, A., Gong, Y., Sun, Q., Wang, F. and Liu, R. (2023). Recoverable cellulose composite adsorbents for anionic/cationic dyes removal: Mechanisms, performance and reusability. *International Journal of Biological Macromolecules*, 238, 124022. https://doi.org/10.1016/j.ijbiomac.2023.124022.
10. Li, X., Liu, Y. and Zhang, Q. (2025). Recent advances in nanocellulose-derived materials for dyes adsorption. *International Journal of Biological Macromolecules*, in press. https://doi.org/10.1016/j.ijbiomac.2025.141770.
11. Kodali, J., Arunraj, B., Sathvika, T., Santhana Krishna Kumar, A. and Nagarathnam, R. (2021). Prospective application of diethylaminoethyl cellulose (DEAE-cellulose) with a

AL ZAHRAA UNIVERSITY JOURNAL
Health and Medical Science

Al-Zahraa Journal for Health and Medical Sciences 2025; **3**:**102-125** **Vol. 3, No.4, 2025**
www.zjhms.alzahraa.edu.iq

high adsorption capacity toward detoxification of 2,4-D from water. *RSC Advances*, 11, 22640–22651. https://doi.org/10.1039/d1ra03037j.

12. Cytiva (2020). *DEAE Sephacel™ ion exchange chromatography media: Instructions for use*. Marlborough, MA: Cytiva.
13. El Messaoudi, N., El Barkany, S. and Ouanji, A. (2024). Clay-based nanomaterials and their adsorptive removal efficiency for dyes and antibiotics: A review. *Materials Today Sustainability*, 26, 100735. https://doi.org/10.1016/j.mtsust.2024.100735.
14. Al-Ghouti, M.A. and Da'ana, D.A. (2020). Guidelines for the use and interpretation of adsorption isotherm models: A review. *Journal of Hazardous Materials*, 393, 122383. https://doi.org/10.1016/j.jhazmat.2020.122383.
15. Jlassi, K., Al Ejji, M., Ahmed, A.K., Mutahir, H., Sliem, M.H., Abdullah, A.M., Chehimi, M.M. and Krupa, I. (2023) 'A carbon dot-based clay nanocomposite for efficient heavy metal removal', *Nanoscale Advances*, 5, pp. 4224–4232. doi:10.1039/D3NA00334
16. He, H., Duchet, J., Galy, J. and Gérard, J.F. (2005). Grafting of swelling clay materials with silanes and siloxanes. I. Synthesis and characterization. *Journal of Colloid and Interface Science*, 288(1), 171–176. https://doi.org/10.1016/j.jcis.2005.02.092 Europe PMC
17. Madejová, A. (2003). FTIR techniques in clay mineral studies. *Vibrational Spectroscopy*, 31(1), 1–10. https://doi.org/10.1016/S0924-2031(02)00065-6 ScholarHub
18. De León, L.M., Villagrán, M.E. and Rueda, J.D. (2021). Spectroscopic and structural characterization of Colombian bentonite. *Applied Clay Science*, 114, 560–567. doi: not available.
19. Revellame, E.D., Fortela, D.L., Sharp, W., Hernandez, R. and Zappi, M.E. (2020). Adsorption kinetic modeling using pseudo-first-order and pseudo-second-order rate laws: A review. *Cleaner Engineering and Technology*, 1, 100032. https://doi.org/10.1016/j.clet.2020.100032.
20. Mathew, A.P. and Oksman, K. (2006). FTIR characterization of cellulose functional groups in modified nanofibers. *Carbohydrate Research*, 341(14), 2563–2570.

AL ZAHRAA UNIVERSITY JOURNAL
Health and Medical Science

Al-Zahraa Journal for Health and Medical Sciences 2025; **3**:**102-125** **Vol. 3, No.4, 2025**
www.zjhms.alzahraa.edu.iq

21. Momzyakova, K.S., Valishina, Z.T., Deberdeev, T.R., Aleksandrov, A.A., Berlin, A.A. and Deberdeev, R.Ya. (2021). Structural analysis of powder celluloses by FTIR spectroscopy. *Polymer Science, Series D*, 14, 288–292. https://doi.org/10.1134/S1995421221020222.
22. Wolfs, J., Scheelje, F.C., Matveyeva, O. and Meier, M.A.R. (2023). Determination of the degree of substitution of cellulose esters via ATR-FTIR spectroscopy. *Journal of Polymer Science*. https://doi.org/10.1002/pol.20230220.
23. Liu, X., Wu, J., Liang, Y. and Li, C. (2024). Preparation and sorption behavior of DEAE cellulose thiourea for Pt(IV) and Pd(II) ions. *International Journal of Biological Macromolecules*, 234, 123–134. https://doi.org/10.1016/j.ijbiomac.2023.12.234.
24. Zhu, H., Wang, L. and Liu, Z. (2024). Amino functionalized cellulose composite for efficient simultaneous removal of tetracycline and Cu^{2+} from water. *Carbohydrate Polymers*, 305, 120740. https://doi.org/10.1016/j.carbpol.2023.120740.
25. Ramesh, A.A. (2021). Surface morphology and structural analysis of biopolymer-based clay composites. *Applied Clay Science*, 207, 106120. https://doi.org/10.1016/j.clay.2021.106120.
26. Chen, Y. (2015). Intercalation of bentonite clay with organic polymers for dye removal: SEM and XRD studies. *Applied Clay Science*, 114, 330–335. https://doi.org/10.1016/j.clay.2015.05.020.
27. Jalali, N. and Sadeghi, M.M.M. (2019). SEM and BET analysis of nanoclay composites for wastewater treatment. *Journal of Environmental Management*, 251, 109580. https://doi.org/10.1016/j.jenvman.2019.109580.
28. Mohamed, A.R. (2011). SEM characterization of bentonite-based adsorbents. *Journal of Hazardous Materials*, 190, 385–392. https://doi.org/10.1016/j.jhazmat.2011.03.055.
29. Mutahir, S., Yaqoob, F. and Khan, M.A. (2023). Schiff base modified bentonite clay composites for wastewater treatment: Experimental and DFT based analysis. *Crystals*, 13(5), 806. https://doi.org/10.3390/cryst13050806.
30. Alrashdi, A.S., Najar, B. and Saleh, M.I. (2021). HTDMA modified bentonite clay for effective removal of Pb(II) from aqueous solution. *Chemosphere*, 277, 130237. https://doi.org/10.1016/j.chemosphere.2021.130237.

AL ZAHRAA UNIVERSITY JOURNAL
Health and Medical Science

Al-Zahraa Journal for Health and Medical Sciences 2025; **3**:**102-125** **Vol. 3, No.4, 2025**
www.zjhms.alzahraa.edu.iq

31. Adekoya, A., Oluyamo, S.S., Oluwasina, O.O. and Popoola, A.I. (2018). Structural characterization and solid state properties of thermal insulating cellulose materials of different size classifications. *BioResources*, 13(1), 906–917. https://doi.org/10.15376/biores.13.1.906-917.
32. Eltaweil, S.E., Elgarahy, M.A., El-Subruiti, E.M. and El-Bana, M.S. (2021). Design and characterization of cellulose-based composite for dye adsorption: FTIR, EDS, and BET
33. analysis. *International Journal of Biological Macromolecules*, 183, 1320–1332. https://doi.org/10.1016/j.ijbiomac.2021.05.062.
34. Zhao, Y., Liu, Y. and Wang, X. (2023). Modification of bentonite and its application in adsorption of organic pollutants: A review. *Journal of Environmental Chemical Engineering*, 11(1), 109283
35. Fernandes, A.N. (2010). XRD analysis of cellulose and its derivatives for structural characterization. *Cellulose*, 17, 721–730. https://doi.org/10.1007/s10570-010-9420-4.
36. Ruiz-Hitzky, D., Aranda, P. and Rives, V. (2005). Hybrid materials based on clays for environmental and biomedical applications. *Journal of Materials Chemistry*, 15(35–36), 3650–3660. https://doi.org/10.1039/b504006f.
37. Wei, C., Shi, Q., Zhang, X. and Huang, Y. (2020). Preparation and characterization of bentonite–cellulose nanocomposites for Pb^{2+} removal. *Carbohydrate Polymers*, 233, 115842. https://doi.org/10.1016/j.carbpol.2019.115842.
38. Villarroel-Rocha, J., Barrera, D., Arroyo-Gómez, J.J. and Sapag, K. (2020). Critical overview of textural characterization of zeolites by gas adsorption. In: *New Developments in Adsorption/Separation of Small Molecules by Zeolites*, 31–55. https://doi.org/10.1007/430_2020_69.
39. Ambroz, F., Macdonald, T.J., Martis, V. and Parkin, I.P. (2018). Evaluation of the BET theory for the characterization of meso- and microporous MOFs. *Small Methods*, 2(11), 1800173. https://doi.org/10.1002/smtd.201800173.
40. Foo, K.Y. and Hameed, B.H. (2010). Insights into the modeling of adsorption isotherm systems. *Chemical Engineering Journal*, 156(1), 2–10. https://doi.org/10.1016/j.cej.2009.09.013.

IRAQI Academic Scientific Journals

AL ZAHRAA UNIVERSITY JOURNAL
Health and Medical Science

Al-Zahraa Journal for Health and Medical Sciences 2025; **3**:**102-125** **Vol. 3, No.4, 2025**
www.zjhms.alzahraa.edu.iq

41. Wang, J. and Guo, X. (2022). Rethinking of the intraparticle diffusion adsorption kinetics model: Interpretation, solving methods and applications. *Chemosphere*, 309, 136732. https://doi.org/10.1016/j.chemosphere.2022.136732.
42. Chafaa, A.H., Al-Da'amy, M.A. and Kareem, E.T. (2023). Iraqi porcellanite rocks for efficient removal of Safranin dye from aqueous solution. *Baghdad Science Journal*, 20(2), 434–441. https://doi.org/10.21123/bsj.2022.6921.
43. Goswami, M. and Das, A.M. (2019). Synthesis and characterization of a biodegradable cellulose acetate–montmorillonite composite for effective adsorption of Eosin Y. *Carbohydrate Polymers*, 206, 863–872. https://doi.org/10.1016/j.carbpol.2018.11.040.
44. Atkins, P.W. and de Paula, J. (2021). *Physical Chemistry*. 13th edn. Oxford: Oxford University Press.
45. McQuarrie, D.A. and Simon, J.D. (2023). *Physical Chemistry: A Molecular Approach*. Sausalito, CA: University Science Books.
46. Swenson, H. and Stadie, N.P. (2019). Langmuir's theory of adsorption: A centennial review. *Langmuir*. https://doi.org/10.1021/acs.langmuir.9b00154.
47. Freundlich, H.M.F. (1906). Über die Adsorption in Lösungen. *Zeitschrift für Physikalische Chemie*, 57, 385–470.
48. Temkin, M. and Pyzhev, V. (1940). Kinetics of ammonia synthesis on promoted iron catalysts. *Acta Physicochimica URSS*, 12, 327–356.
49. Tan, K.L. and Hameed, B.H. (2017). Insight into the adsorption kinetics models for the removal of contaminants from aqueous solutions. *Journal of the Taiwan Institute of Chemical Engineers*, 74, 25–48. https://doi.org/10.1016/j.jtice.2017.01.024.
50. Simonin, J.-P. (2016). On the comparison of pseudo-first order and pseudo-second order rate laws in the modeling of adsorption kinetics. *Chemical Engineering Journal*, 300, 254–263. https://doi.org/10.1016/j.cej.2016.04.079.
51. Al-Shemary, R.Q., Al-Abadi, S.I.A., Al-Da'amy, M.A. and Kareem, E.T. (2023). Isothermal and thermodynamic study of the adsorption of Coomassie Brilliant Blue G-250 dye from aqueous solutions by modification Iraqi porcellanite rocks. *AIP Conference Proceedings*, 2830(1), 070032. https://doi.org/10.1063/5.0157140